

RSC Advances



This is an *Accepted Manuscript*, which has been through the Royal Society of Chemistry peer review process and has been accepted for publication.

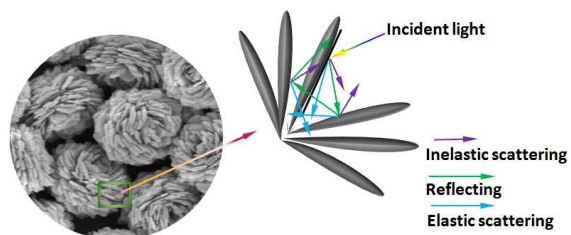
Accepted Manuscripts are published online shortly after acceptance, before technical editing, formatting and proof reading. Using this free service, authors can make their results available to the community, in citable form, before we publish the edited article. This *Accepted Manuscript* will be replaced by the edited, formatted and paginated article as soon as this is available.

You can find more information about *Accepted Manuscripts* in the [Information for Authors](#).

Please note that technical editing may introduce minor changes to the text and/or graphics, which may alter content. The journal's standard [Terms & Conditions](#) and the [Ethical guidelines](#) still apply. In no event shall the Royal Society of Chemistry be held responsible for any errors or omissions in this *Accepted Manuscript* or any consequences arising from the use of any information it contains.

Graphical abstract

(BiO)₂CO₃ hierarchical microspheres showed higher visible light photocatalytic activity due to enhanced extrinsic absorption benefiting from light reflecting and scattering.



Cite this: DOI: 10.1039/c0xx00000x

www.rsc.org/xxxxxx

Communication

Enhanced extrinsic absorption promotes the visible light photocatalytic activity of wide band-gap (BiO)₂CO₃ hierarchical structureTing Xiong^a, Fan Dong^{a*}, Zhongbiao Wu^{b*}

Received (in XXX, XXX) Xth XXXXXXXXX 20XX, Accepted Xth XXXXXXXXX 20XX

DOI: 10.1039/b000000x

(BiO)₂CO₃ hierarchical microspheres and (BiO)₂CO₃ nanoparticles with wide band-gaps were fabricated by a simple hydrothermal method. The former showed higher visible light photocatalytic activity towards removal of NO than the latter due to the enhanced extrinsic absorption benefiting from the strong light reflecting and scattering effects. The extrinsic absorption over (BiO)₂CO₃ hierarchical microspheres can induce the production of holes and electrons with visible light, subsequently generating active species to participate in photocatalytic reactions.

Research of semiconductor materials with different morphology and dimensions has been an active area over the last decades because of their shape and size dependent physical, chemical, electronic, and optical properties.¹ Especially, materials with three dimensional (3D) hierarchical structure attracted considerable attention due to their widespread potential applications in biology, drugs delivery, photovoltaics, lithium ion storage, catalysis, photocatalysis, sensors and supercapacitors.²

Recently, 3D structured semiconductor photocatalysts have been under intensively investigated because of their efficient photocatalytic activity resulting from the large surface areas, special pore structure, efficient light harvesting and charge separation.³ For wide band-gap semiconductors, they are restricted by their deficient visible light absorption. Many efforts have been devoted to overcoming this bottom neck, centring mainly on the improvement of intrinsic absorption (electron transitions from the valance band to conduction band of a semiconductor).^{4,5} Most recently, fabrication of 3D structures are reported to be an effective way to boost the visible light absorption of wide band-gap semiconductors due to the reflecting and scattering effects. For example, Que's group synthesized TiO₂ microspheres with enhanced visible light absorption and photocatalytic activity compared with P25 although it is involved with the doping of F atom.⁶ Liu et al. fabricated hierarchical hollow TiO₂ spheres with improved visible light photocatalytic activity towards degradation of RhB.⁷ Likewise, Lu and co-workers prepared BiOCl hierarchical nanostructures with enhanced visible light photocatalytic properties.⁸ Yet, little is known about how the reflecting and scattering effects improve the visible light absorption and the corresponding photocatalytic activities of wide band-gap semiconductors.

(BiO)₂CO₃, a typical wide band-gap semiconductor, displaying promising antibacterial, sensing, super capacitor, and

photocatalysis performance, draws increasing research interests.⁹ Herein, (BiO)₂CO₃ hierarchical microspheres (BOC-R3) and (BiO)₂CO₃ nanoparticles (BOC-R6) were fabricated by hydrothermal treatment of bismuth citrate and sodium carbonate via adjusting the dosage of precursors. The as-prepared samples were utilized to photocatalytic removal of NO under both visible and UV light. Except the phenomenon that BOC-R3 showed higher UV light photocatalytic activity than BOC-R6. We found that BOC-R3 displayed enhanced visible light photocatalytic activity compared to BOC-R6. The enhanced visible light photocatalytic activity is supposed to be associated with the improved extrinsic absorption (such as impurity, the excitation of surface states and the photoionization of defects) originating from the strong light reflecting and scattering effects of incident photons in the 3D hierarchical structure. The improved extrinsic absorption can induce free electrons and holes to initiate chemical reactions. This work, in terms of the enhanced visible light absorption and activity of wide band-gap semiconductors with 3D hierarchical structures, provides new insights and sheds light on the dominant role of extrinsic absorption.

The detailed procedure for the experiments was described in ESI. XRD patterns of the BOC-R3 and BOC-R6 samples are shown in Fig. 1a. All diffraction peaks of the two samples could match the orthorhombic (BiO)₂CO₃ crystallites (JCPDS file No. 25-1464). XPS survey spectra in Fig. 1b demonstrate that the two samples only contain Bi, O and C elements, further confirming that the two samples are pure (BiO)₂CO₃. The XPS spectra of Bi, O and C elements shown in Fig. S1 (detailed discussions in ESI[†]) suggest that each corresponding element in the two samples has similar chemical environment. In addition, four characteristic bands in FT-IR (Fig. S2 (ESI[†])) at ν₁ (1067 cm⁻¹), ν₂ (846 and 820 cm⁻¹), ν₃ (1468 and 1391 cm⁻¹), ν₄ (670 cm⁻¹), ν₁+ν₄ (1756 and 1730 cm⁻¹) corresponding to the internal vibrations of "free" CO₃²⁻ can be observed in the two samples, respectively.¹⁰

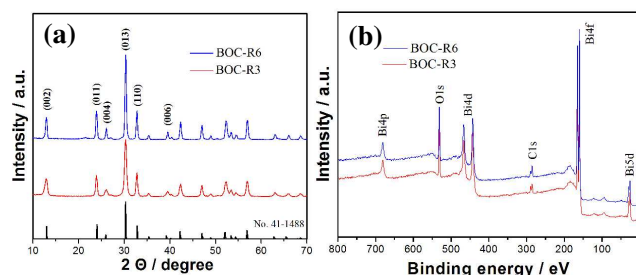


Fig. 1 XRD patterns (a) and XPS survey spectra (b) of the BOC-R3 and BOC-R6 samples.

Fig. 2 and Fig. 3 present the SEM and TEM images of the as-prepared samples. From low-magnification SEM image of the BOC-R3 sample (Fig. 2a), we can observe many isolated uniform microspheres with a diameter of ~ 1.3 μm . These BOC-R3 microspheres are constructed by dozens of nanosheets with a thickness ranging from 20.9 to 44.8 nm. Meantime, many pores are formed among the self-assembled nanosheets. The TEM image (Fig. 2b) shows that the entire microsphere contains a hollow in the center. An HRTEM image of a single nanosheet in the microsphere is displayed in Fig. 2c. The measured lattice spacing is about 0.295 nm, which agrees well with the d-spacing of (013) crystal face of $(\text{BiO})_2\text{CO}_3$. The SAED pattern (Fig. 2d) displays an array of clear and regular diffraction spots of one single nanosheet, indicating that the nanosheet is well-defined single crystalline. Furthermore, the results of EDX analysis indicate the presence of Bi, O and C elements in BOC-R3, confirming that the sample is of high purity (Fig. S3 (ESI[†])).

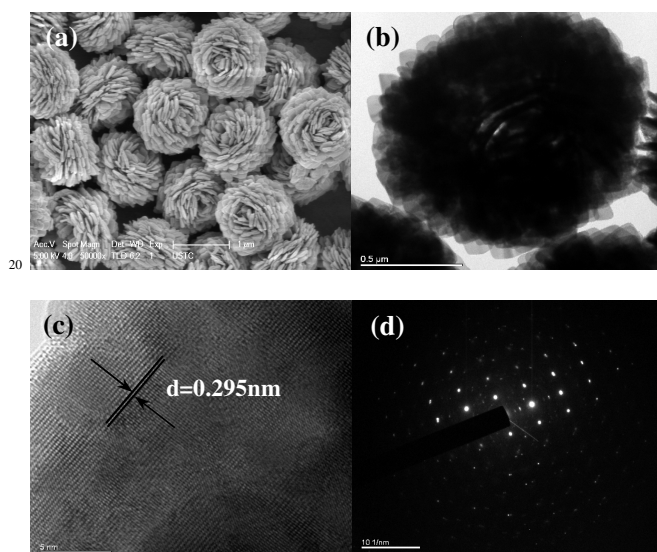


Fig. 2 SEM (a) and TEM (b and c) images of the as-prepared BOC-R3 sample, SAED (d) of a single nanosheet.

In contrast, the BOC-R6 samples with nanoparticles morphology are prepared though increasing the concentration of CO_3^{2-} (Fig. 3a). These nanoparticles with thickness being 71.6–277 nm are not uniform. Further observation in Fig. 3b also shows that these nanoparticles are irregular. The excessive CO_3^{2-} not only induces the preferred growth orientation, generating nanoparticles with increasing thickness, but also accelerates the reaction process, making both nucleation and growth be a kinetic control. Naturally, irregular nanoparticles are achieved. Fig. 3c displays the HRTEM image of an individual nanoparticle. The clear lattice fringes with an interplanar lattice spacing of 0.273 nm correspond to the (110) atomic planes. The corresponding SAED pattern (Fig. 3d) indicates the single-crystalline characteristic of the $(\text{BiO})_2\text{CO}_3$ nanoparticles. The specific surface areas of BOC-R3 and BOC-R6 were determined to be 13.8 and 3.1 m^2/g , respectively. The pore size distribution curve

of BOC-R3 displays a pore size distribution centered at ca. 30 nm, which confirmed that the BOC-R3 samples are mesoporous (Fig. S4 (ESI[†])). And BOC-R6 exhibits a pore size distribution range < 2 nm, indicating that the BOC-R6 samples are microporous (Fig. S4 (ESI[†])).

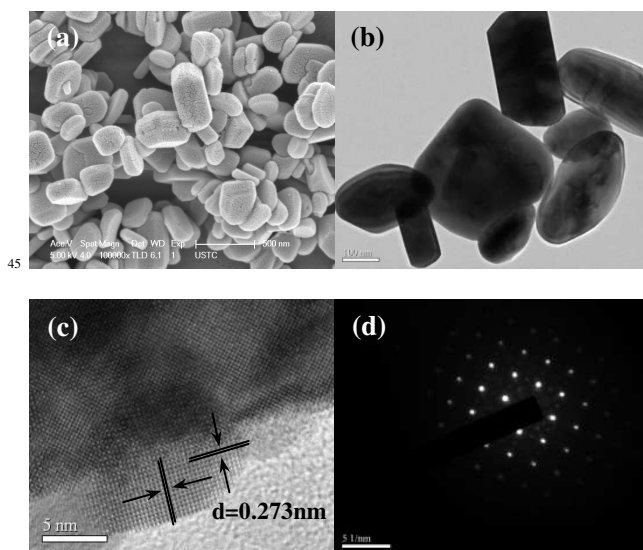


Fig. 3 SEM (a) and TEM (b and c) images of the as-prepared BOC-R6 sample, SAED (d) of a single nanoparticle.

As seen from Fig. 4, BOC-R3 and BOC-R6 exhibit strong absorptions with a steep edge at ca. 365 nm, and BOC-R3 exhibits enhanced UV light absorption compared with BOC-R6. The 3D structure doesn't cause obvious shift in the fundamental absorption edge of $(\text{BiO})_2\text{CO}_3$. Notably, BOC-R3 shows certain light absorption in the visible region while BOC-R6 doesn't. As known to all, light reflecting and scattering effects are obvious in 3D nanostructure. On one hand, the incident light can reach the place though reflecting and scattering where the incident cannot directly achieve, and subsequently increase the absorption probability. On the other hand, it is well-known that the energy of light will be reduced after multiple inelastic scatterings. The semiconductors in reality are extrinsic semiconductors. Except for the intrinsic light absorption, the semiconductor owns extrinsic absorptions including the photoionization of defects absorption, the excitation of surface states absorption, and defects or impurity absorption, which absorb lower energy than the intrinsic absorption.¹¹

In the UV light region, the absorptions of the two samples are caused by vast intrinsic absorptions and minor extrinsic absorptions. Due to the strong light reflecting and scattering effects, the BOC-R3 sample exhibits high UV light absorption compared to BOC-R6. Nevertheless, in the visible light region, the energy of the light is too low to induce the intrinsic absorption of the two samples due to the large band gaps (the band gaps of the as-synthesized BOC-R3 and BOC-R6 (E_g) samples estimated from the intercept of the tangents to the plots of $(\text{Ah}\nu)^{1/2}$ vs. photo energy were 3.34 and 3.41 eV, respectively (inset of Fig. 4)). Thus, the visible light absorption stems from extrinsic absorption. The strong reflecting and scattering effects in BOC-R3 make BOC-R3 possess visible light absorption, but BOC-R6 shows

ignorable visible light absorption because of its weak reflecting and scattering effects. The schematic diagram of the reflecting and scattering effects of incident light in $(\text{BiO})_2\text{CO}_3$ hierarchical microspheres structure is shown in Fig. 5. Fig. S5a (ESI[†]) shows the PL spectra of the two samples with an exciting wavelength of 430 nm. It can be seen that BOC-R3 and BOC-R6 samples exhibit a strong PL signal with a obvious PL peak at about 498 and 503 nm, respectively. Since the intrinsic band transition with 430 nm light is impossible, the PL peak around 500 nm suggests that defects exist in the crystal structure of the two samples (Fig. S5b).

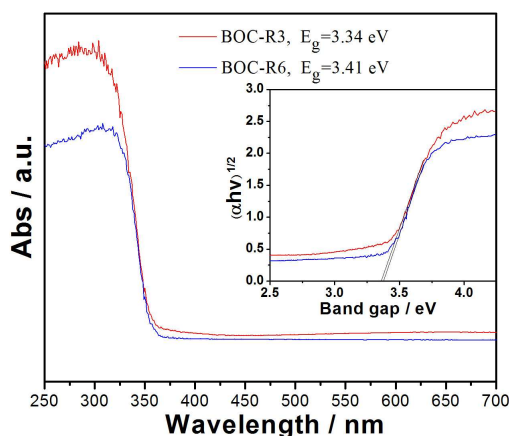


Fig. 4 UV-vis DRS of the two samples.

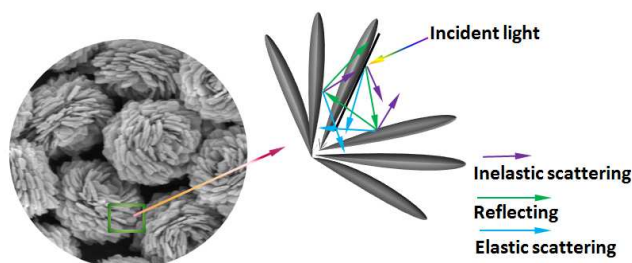


Fig. 5 Schematic diagram of the reflecting and scattering effects in $(\text{BiO})_2\text{CO}_3$ hierarchical microspheres.

Afterwards, we tested the photoelectrochemical performance of the two samples under visible light as shown in Fig. 6. BOC-R3 sample shows the transient photocurrent responses under visible light irradiation, which implies that the light absorbed by extrinsic absorption could induce the production of holes and electrons, while BOC-R6 displays very low photocurrent responses mainly due to its weak extrinsic absorption (Fig. 6a). The Electrochemical impedance spectroscopy (EIS) is used to investigate the photogenerated charge separation process as shown in Fig. 6b. The diameter of the arc radius on the EIS Nyquist plot of BOC-R3 is smaller than that of BOC-R6 under visible light irradiation, which suggests an effective separation of photogenerated electron-hole pairs and fast interfacial charge transfer due to the special hierarchical nanosheets structure of BOC-R3.

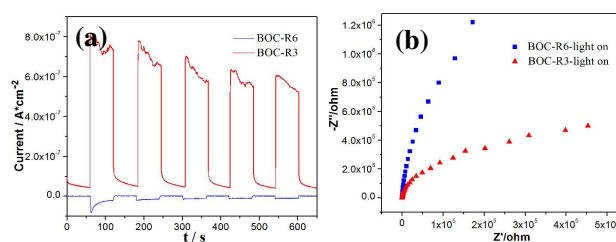


Fig. 6 Photocurrent-time curves (a) and electrochemical impedance spectroscopy spectra (b) of BOC-R3 and BOC-R6 samples under visible light irradiation.

To confirm their photocatalytic activity, the two samples were evaluated by photocatalytic removal of NO in air. Firstly, we investigated the photocatalytic activity of the two samples under UV (360nm) light irradiation. The 360nm light photolysis of NO can be negligible without photocatalyst.¹² As displayed in Fig. S6a (ESI[†]), the removal ratios of NO by BOC-R3 and BOC-R6 products are 42.8% and 25.2%, respectively. In the UV light region, the samples possess intrinsic absorption and extrinsic absorption. The intrinsic light absorption induces electron transitions from the valance band to conduction band to produce free electrons and holes. The extrinsic absorption also can produce free electrons and holes to take part in the photocatalytic reaction as well.¹³ The strong reflecting and scattering of light in BOC-R3 result in high UV light activity. The reaction rate constant k_{UV} of BOC-R3 is $(15.3 \times 10^{-2} \text{ min}^{-1})$ higher than that of BOC-R6 $(10.4 \times 10^{-2} \text{ min}^{-1})$ as shown in Fig. S6b (ESI[†]). Also, the normalized rate constants k'_{UV} was calculated and the result was given in table 1. Notably, the BOC-R3 shows lower k'_{UV} than BOC-R6, this phenomenon may be associated with the poor extrinsic absorptions compared with the intrinsic absorptions in the UV region. Anyhow, BOC-R3 showed higher UV light photocatalytic activity than BOC-R6 although surface area plays a major role on the photocatalytic activity in the UV region.

Then, the photocatalytic activities over BOC-R3 and BOC-R6 samples under visible light irradiation with different wavelength were studied. The visible light photolysis of NO can be ignorable without photocatalyst according to the previous research.¹² when a 420 nm cut-off filter was used, from Fig. 7a, we find that BOC-R3 shows a removal ratio of 23%, while BOC-R6 shows negligible visible light activity. This result reveals that the photoexcitation by extrinsic absorption can generate free charge carriers which can take part in chemical reactions, consistent with the finding reported by Serpone et al. who have studied the photoadsorption of H_2 , CH_4 (donor) and O_2 (acceptor) molecules on the surface of wide band-gap metal oxides and concluded that photoreaction can be caused by the photoexcitation of extrinsic absorption of a catalyst.¹³ Moreover, the reaction rate constant k_{vis} of BOC-R3 is $7.6 \times 10^{-2} \text{ min}^{-1}$, which is about 19 times of BOC-R6 $(0.4 \times 10^{-2} \text{ min}^{-1})$ as shown in Fig. 7b. The normalized rate constants k'_{vis} was calculated as shown in table 1. The BOC-R3 $(5.5 \times 10^{-3} \text{ min}^{-1})$ also shows higher k'_{vis} than BOC-R6 $(1.3 \times 10^{-3} \text{ min}^{-1})$. Obviously, BOC-R3 displays high reaction rate. In addition, the reaction intermediate of NO_2 during photocatalytic oxidation of NO under UV light and visible light is monitored online as shown in Fig. 8. The fraction of NO_2 generated over BOC-

R3 is lower than that with BOC-R6 whether it is under UV light or visible light irradiation. Namely, BOC-R3 promotes the oxidation of intermediate NO_2 to final NO_3^- product. We also used a cut-off filter with 450 nm and 510 nm to test the photocatalytic activity, respectively (Fig. S7 (ESI[†])). Similarly, BOC-R3 shows higher activity than BOC-R6. Furthermore, the long-term visible (>420 nm) photocatalytic activity of BOC-R3 was performed (Fig. 9). Obviously, there is no obvious deactivation in the removal of NO even after 17 h of visible light irradiation, which indicates the stable and efficient photocatalytic activity of BOC-R3 sample.

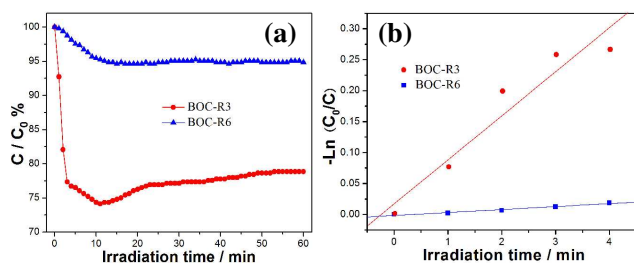


Fig. 7 Photocatalytic activity toward removal of NO under visible light irradiation (a) and reaction rate constants k_{vis} (b) of the BOC-R3 and BOC-R6 samples

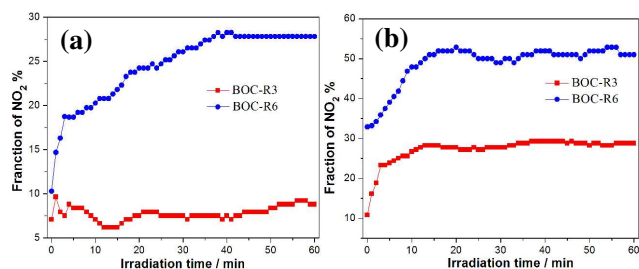


Fig. 8 Monitoring of NO_2 intermediates during UV light irradiation (a) and visible light irradiation (b).

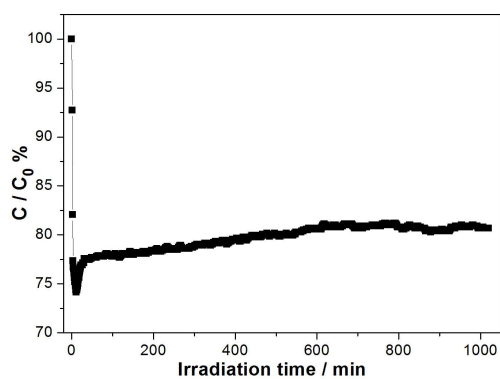


Fig. 9 Long-term photocatalytic activity of BOC-R3 under visible light irradiation (>420 nm).

ESR spectra were carried out under visible light irradiation in aqueous dispersion for DMPO- $\bullet\text{OH}$ (Fig. 10). As displayed in Fig. 10a, the characteristic peaks of DMPO- $\bullet\text{OH}$ can be observed in BOC-R3 under light illumination, indicating the generation of

$\bullet\text{OH}$ radicals. Such result indicates that the photogenerated carriers produced via extrinsic absorption further induce the production of active species. However, nearly no sign of $\bullet\text{OH}$ radicals can be observed over BOC-R6 (Fig. 10b). The low visible light absorption and then the ignorable production of holes and electrons are responsible for the poor activity. Therefore, we can conclude that the enhanced extrinsic absorptions of BOC-R3 can produce free electrons and holes to take part in the photocatalytic reaction. The high photocatalytic activity of BOC-R3 is directly related to the 3D structure. The special 3D structure allows multiple reflecting and scattering of incident visible light, which will increase the extrinsic absorption. Also, the 3D hierarchical structure is favourable for the diffusion of reaction intermediates and thus accelerating the reaction rate. Namely, the 3D structures enhance the light-harvesting efficiency and increase the quantity of photogenerated carriers to participate in the photocatalytic reaction, consequently dramatically enhancing the visible light photocatalytic activity. Besides, this result also suggests that the visible light photocatalytic activity of wide band-gap semiconductors with 3D hierarchical structure mainly arises from the extrinsic absorption.

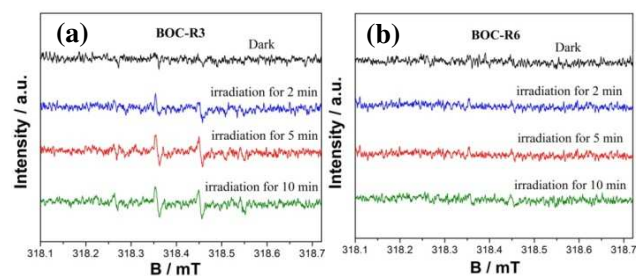


Fig. 10 DMPO spin-trapping ESR spectra of BOC-R3 (a) and BOC-R6 (b) in aqueous dispersion for DMPO- $\bullet\text{OH}$.

Table 1 Physicochemical properties, Reaction rate constants k and Normalized rate constants k' of BOC-R3 and BOC-R6 samples.

Samples	S_{BET} (m^2/g)	$k_{\text{UV}}(\times 10^7)$ min^{-1}	$k'_{\text{UV}}(\times 10^7)$ min^{-1}	$k_{\text{vis}}(\times 10^7)$ min^{-1}	$k'_{\text{vis}}(\times 10^7)$ min^{-1}
BOC-R3	13.8	15.3	11.1	7.6	5.5
BOC-R6	3.1	10.4	33.6	0.4	1.3

In summary, $(\text{BiO})_2\text{CO}_3$ hierarchical microspheres and $(\text{BiO})_2\text{CO}_3$ nanoparticles were fabricated by hydrothermal treatment of bismuth citrate and sodium carbonate by tuning the molar ratio of the precursors. The fabricated samples were applied to photocatalytic removal of NO in air under both UV and visible light. The results indicate that $(\text{BiO})_2\text{CO}_3$ hierarchical microspheres not only showed high UV light photocatalytic activity but also displayed enhanced visible light photocatalytic activity in comparison with $(\text{BiO})_2\text{CO}_3$ nanoparticles. The enhanced visible light photocatalytic activity can be attributed to the increased extrinsic absorption originating from the strong reflecting and scattering effects of incident light in 3D structure. The present work is expected to shed new light on the understanding of enhanced visible light photocatalytic activity of

wide band-gap semiconductors mediated by light reflecting and scattering effects in 3D structure. This work could also provide a new perspective for the designed synthesis of visible light photocatalysts by controlling the internal structure of the materials.

This research is financially supported by the National Natural Science Foundation of China (51108487, 51478070), the National Science Foundation Project of CQ CSTC (cstc2013jcyjA20018), and the Innovative Research Team Development Program in University of Chongqing (KJTD201314).

Notes and references

- ^a Chongqing Key Laboratory of Catalysis and Functional Organic Molecules, College of Environmental and Biological Engineering, Chongqing Technology and Business University, Chongqing, 400067, China.
- ^b Department of Environmental Engineering, Zhejiang University, Hangzhou 310027, PR China
- * To whom correspondence should be addressed.
E-mail: djctbu@126.com (Fan Dong), zbwu@zju.edu.cn (Zhongbiao Wu).
Tel.: +86-23-62769785-605; Fax: +86-23-62769785-605.
- [†] Electronic supplementary information (ESI) available: Experimental details, characterization, and Fig. S1 to S7. See DOI: 10.1039/b000000x/
- 1 (a) H. Goesmann and C. Feldmann, *Angew. Chem. Int. Ed.*, 2010, **49**, 2; (b) M. S. Xu, T. Liang, M. M. Shi and H. Z. Chen, *Chem. Rev.*, 2013, **113**, 3766; (c) X. Y. Lai, J. E. Halpert and D. Wang, *Energy Environ. Sci.*, 2012, **5**, 5604; (d) Y. Hu, X. H. Gao, L. Yu, Y. L. Wang, J. Q. Ning, S. J. Xu and X. W. Lou, *Angew. Chem. Int. Ed.*, 2013, **52**, 5636-5639; (e) L. Zhang and Y. Zhu, *Catal. Sci. Technol.*, 2012, **2**, 694-706; (f) K. Zhang and L. Guo, *Catal. Sci. Technol.*, 2013, **3**, 1672-1690.
- 2 (a) M. P. Melancon, M. Zhou and C. Li, *Acc. Chem. Res.*, 2011, **44**, 947; (b) M. D'Arienzo, L. Armelao, A. Cacciamani, C. M. Mari, S. Polizzi, R. Ruffo, R. Scotti, A. Testino, L. Wahba and F. Morazzoni, *Chem. Mater.*, 2010, **22**, 4083; (c) Y. Ma, G. Ji, B. Ding and J. Y. Lee, *J. Mater. Chem.*, 2012, **22**, 24380; (d) L. W. Zhang, T. G. Xu, X. Zhao and Y. F. Zhu, *Appl. Catal. B.*, 2010, **98**, 138; (e) M. Zhou, H. B. Wu, J. Bao, L. Liang, X. W. Lou and Y. Xie, *Angew. Chem. Int. Ed.*, 2013, **52**, 8679; (f) B. F. Machado and P. Serp, *Catal. Sci. Technol.*, 2012, **2**, 54-75; (g) A. Chithambararaj, N. S. Sanjini, A. Chandra Bose and S. Velmathi, *Catal. Sci. Technol.*, 2013, **3**, 1405-1414.
- 3 (a) J. W. Shi, J. H. Ye, Q. Y. Li, Z. H. Zhou, H. Tong, G. C. Xi and L. J. Guo, *Chem. Eur. J.*, 2012, **18**, 3157; (b) Y. S. Jun, J. Park, S. U. Lee, A. Thomas, W. H. Hong and G. D. Stucky, *Angew. Chem. Int. Ed.*, 2013, **52**, 1; (c) Z. Sun, J. H. Kim, Y. Zhao, F. Bijarbooneh, V. Malgras, Y. Lee, Y.-M. Kang and S. X. Dou, *J. Am. Chem. Soc.*, 2011, **133**, 19314.
- 4 (a) T. Zhou, Y. Du, A. Borgna, J. Hong, Y. Wang, J. Han, W. Zhang and R. Xu, *Energy Environ. Sci.*, 2013, **6**, 3229-3234; (b) W.-J. Ong, L.-L. Tan, S.-P. Chai, S.-T. Yong and A. R. Mohamed, *Nano Research*, 2014, DOI: 10.1007/s12274-014-0514-z; (c) J. Ran, J. Zhang, J. Yu, M. Jaroniec and S. Z. Qiao, *Chem. Soc. Rev.*, 2014, DOI: 10.1039/C3CS60425J; (d) L. Liu, Z. Liu, A. Liu, X. Gu, C. Ge, F. Gao and L. Dong, *ChemSusChem*, 2014, **7**, 618-626.
- 5 (a) X. B. Chen and C. Burda, *J. Am. Chem. Soc.*, 2008, **130**, 5018; (b) H. J. Huang, D. Z. Li, Q. Lin, W. J. Zhang, Y. Shao, Y. B. Chen, M. Sun and X. Z. Fu, *Environ. Sci. Technol.*, 2009, **43**, 4164; (c) F. Dong, T. Xiong, R. Wang, Y. J. Sun and Y. K. Jiang, *Dalton Trans.*, 2014, **43**, 6631.
- 6 Z. L. He and W. X. Que, *Phys. Chem. Chem. Phys.*, 2013, **15**, 16768.
- 7 G. L. Li, H. Y. Zhang, J. Lan, J. Li, Q. W. Chen, J. Y. Liu and G. B. Jiang, *Dalton Trans.*, 2013, **42**, 8541.
- 8 J. Y. Xiong, Z. B. Jiao, G. X. Lu, W. Ren, J. H. Ye and Y. P. Bi, *Chem. Eur. J.*, 2013, **19**, 9472.
- 9 (a) G. Cheng, H. M. Yang, K. F. Rong, Z. Lu, X. L. Yu and R. Chen, *J. Solid State Chem.*, 2010, **183**, 1878; (b) F. Qin, G. F. Li, R. M. Wang, J. L. Wu, H. Z. Sun and R. Chen, *Chem. Eur. J.*, 2012, **18**, 16491; (c) F. Dong, W.-K. Ho, S. C. Lee, Z. B. Wu, M. Fu, S. C. Zou and Y. Huang, *J. Mater. Chem.*, 2011, **21**, 12428; (d) S. Peng, L. Li, H. Tan, Y. Wu, R. Cai, H. Yu, X. Huang, P. Zhu, S. Ramakrishna, M. Srinivasan and Q. Yan, *J. Mater. Chem. A*, 2013, **1**, 7630; (e) P. Madhusudan, J. Zhang, B. Cheng and G.

- Liu, *CrystEngComm*, 2013, **15**, 231; (f) X. Zhang, Y. Zheng, D. G. McCulloch, L. Y. Yeo, J. R. Friend and D. R. MacFarlane, *J. Mater. Chem. A*, 2014, **2**, 2275; (g) Y. Zhang, D. Li, Y. Zhang, X. Zhou, S. Guo and L. Yang, *J. Mater. Chem. A*, 2014, **2**, 8273.
- 10 G. E. Tobon-Zapata, S. B. Etcheverry and E. J. Baran, *J. Mater. Sci. Lett.*, 1997, **16**, 656.
- 11 (a) V. Ryabchuk, *Int. J. Photoenergy*, 2004, **6**, 95-113; (b) M. V. Ganduglia-Pirovano, A. Hofmann and J. Sauer, *Surf. Sci. Rep.* 2007, **62**, 219-270; (c) A. V. Emeline, G. V. Kataeva, V. K. Ryabchuk and N. Serpone, *J. Phys. Chem. B.*, 1999, **103**, 9190. (d) X. Pan, M.-Q. Yang, X. Fu, N. Zhang and Y.-J. Xu, *Nanoscale*, 2013, **5**, 3601-3614.
- 12 F. Dong, A. M. Zheng, Y. J. Sun, M. Fu, B. Q. Jiang, W. K. Ho, S. C. Lee and Z. B. Wu, *CrystEngComm*, 2012, **14**, 3534.
- 13 (a) A. V. Emeline, K. R. Vladimirov and N. Serpone, *J. Phys. Chem. B.*, 1991, **103**, 1316; (b) A. V. Emeline, G. N. Kuzmin, D. Purevdorj, V. K. Ryabchuk and N. Serpone, *J. Phys. Chem. B.*, 2000, **104**, 2989.